

Article

Jet Impingement Cooling Enhanced with Nano-Encapsulated PCM

Mohammad Reza Mohaghegh *, Syeda Humaira Tasnim, Amir A. Aliabadi and Shohel Mahmud

School of Engineering, University of Guelph, Guelph, ON N1G 2W1, Canada; stasnim@uoguelph.ca (S.H.T.); aaliabad@uoguelph.ca (A.A.A.); smahmud@uoguelph.ca (S.M.)

* Correspondence: mohaghem@uoguelph.ca

Abstract: In the present study, the laminar flow and heat transfer of water jet impingement enhanced with nano-encapsulated phase change material (NEPCM) slurry on a hot plate is analytically investigated for the first time. A similarity solution approach is applied to momentum and energy equations in order to determine the flow velocity and heat transfer fields. The effect of different physical parameters such as jet velocity, Reynolds number, jet inlet temperature, and the NEPCM concentration on the cooling performance of the impinging jet are investigated. The volume fraction of NEPCM particles plays an essential role in the flow and heat transfer fields. The results show that NEPCM slurry can significantly enhance the cooling performance of the system as it improves the latent heat storage capacity of the liquid jet. However, the maximum cooling performance of the system is achieved under an optimum NEPCM concentration (15%). A further increase in NEPCM volume fraction has an unfavorable effect due to increasing the viscosity and reducing the conductivity simultaneously. The effect of adding nano-metal particles on the heat transfer performance is also investigated and compared with NEPCM slurry. NEPCM slurry shows a better result in its maximum performance. Compared with the water jet, adding nano and NEPCM particles would overall enhance the system's thermal performance by 16% and 7%, respectively.

Keywords: jet impingement cooling; nano-encapsulated phase change material; similarity solution; heat transfer; optimization



Citation: Mohaghegh, M.R.; Tasnim, S.H.; Aliabadi, A.A.; Mahmud, S. Jet Impingement Cooling Enhanced with Nano-Encapsulated PCM. *Energies* **2022**, *15*, 1034. <https://doi.org/10.3390/en15031034>

Academic Editors: Mahdi Alipour, Majid Khazaei, Komeil Kohansal Sadetmahaleh, Hosein Gholami-Khesht and Mohammad Alipour

Received: 16 December 2021

Accepted: 27 January 2022

Published: 29 January 2022

Publisher's Note: MDPI stays neutral with regard to jurisdictional claims in published maps and institutional affiliations.



Copyright: © 2022 by the authors. Licensee MDPI, Basel, Switzerland. This article is an open access article distributed under the terms and conditions of the Creative Commons Attribution (CC BY) license (<https://creativecommons.org/licenses/by/4.0/>).

1. Introduction

Jet impingement cooling (JIC) is a highly efficient technique in heat treatment, thermal management, and cooling of hot surfaces [1]. With relatively simple equipment but the ability to extract high heat flux, this technology is widely used in many industrial applications such as cooling of electronic chips and microelectronic circuits, nuclear power plants, and hot rolling steel strip [2,3]. The impinging jets are categorized in five different configurations, i.e., free surface jet, plunging jet, submerged jet, confined jet, and wall jet [4]. Free surface jet configuration is considered to be a major classification of JIC [5–7]. In this configuration, a fluid jet (usually water) exits from a nozzle into an ambient gas (mostly air) and impinges on the target surface. Depending on the phase of coolants or the state of jet flow, free surface jets can be distinguished in single- and two-phase JIC. Single-phase impinging jets have been studied extensively, experimentally and numerically, by various researchers, e.g., [8–15]. A comprehensive review of the single-phase JIC technique and its heat transfer methods has recently been conducted by Ekkad et al. [2]. They reviewed a variety of modifications and applications of the JIC technique focusing on impacting novel design, implementation, and improved manufacturing techniques for heat transfer enhancement. In another recent review study, experimental works on the impingement of multiple liquid jets (arrays of impinging jets) on flat surfaces are reviewed by [16].

Two-phase JIC can refer to jet impingement boiling (JIB [3]) in which the impinging liquid is allowed to boil on a hot surface ([4,17–26]) or jet flow is itself in the two-phase

form such as dusty flow jets, e.g., [27]. A comprehensive review of the jet impingement boiling has been published by Wolf et al. [4]. Recently, Mohaghegh et al. [1,3,6] presented a mechanistic model with a similarity solution approach to simulate the jet impingement boiling. Two-phase flow jets such as nanofluids and dusty fluids have been investigated by several researchers. They can be treated as one or two separated phases. Mohaghegh et al. [27] simulated a three-dimensional stagnation-point flow and heat transfer of a dusty fluid toward a stretching sheet. They investigated the effect of non-axisymmetric velocity components on the surface (velocity ratio), fluid and thermal particle interaction parameters, and stretching sheet velocity parameters on the fluid and heat transfer fields. Considering the interaction of phases in the form of source terms in the governing equations, they employed the conservation equations for each phase separately.

Under a creation condition and concentration of the second phase dispersed in the base liquid, the two-phase flow can be treated as a single phase, but the effect of the second phase can be considered as effective thermophysical properties of the mixture (e.g., a homogeneous flow including carried fluid (base fluid) and dispersed particles). Nanofluid simulations in the literature are good examples of this kind of flow. A recent review study on nanofluid jet impingement cooling is provided by Tyagi et al. [28]. They provided an overview of studies conducted on nanofluid spray/jet impingement cooling with a focus on the jet nozzle and surface configuration such as the nozzle to plate distance, plate inclination, and the surface roughness, and the flow parameters such as jet Reynolds and Prandtl numbers.

Improving the thermophysical properties of the base coolant by adding nanoparticles is an effective method to enhance the thermal efficiency of JIC. The majority of this improvement is associated with thermal conductivity and specific heat capacity of the advanced coolant [29]. Metallic nanoparticles used in nanofluid JIC referred earlier enhance the thermal conductivity of the coolant, while nano-encapsulated phase change material (NEPCM) particles dispersed in the base liquid coolant known as NEPCM slurry are proposed to improve the heat capacity of the base coolant [29]. Wu et al. [30] experimentally investigated the effect of adding NEPCM particles in water to enhance the performance of jet impingement and spray cooling. They concluded that the NEPCM slurry can enhance the heat transfer coefficient significantly compared to pure water jet impingement and spray cooling, respectively. Rehman et al. [31] numerically investigated the thermal performance of free-surface jet impinging cooling using NEPCM slurry. They employed a commercial computational fluid dynamics (CFD) code FLUENT to simulate the problem in a fully turbulent regime.

A thorough review of the literature reveals that most studies on JIC have been carried out with the single-phase, mostly air and water, while very few studies are reported on JIC with NEPCM slurry as coolant. The existing experimental works are limited by providing a small range of data, under a certain or a small range of physical parameter variations, which leads to reporting some empirical constants or fitting parameters which may not be valid for other conditions. On the other hand, the existing two-phase numerical models based on CFD or DNS simulations are very costly in solving details of phase change with not much progress in giving accurate results. The numerical simulation of jet impingement flow also involves several complexities, such as free-surface tracking.

In this work, JIC enhanced with NEPCM is studied. The similarity solution approach is proposed to simulate the flow and heat transfer field. Appropriate similarity variables for governing equations are derived for the current problem. To avoid the complexities that correspond with the interactions between two phases (particle-fluid interaction), the effective thermophysical property approach is proposed and used in the governing equation. To the best of our knowledge, no attempts have been made to analyze jet impingement cooling enhanced with NEPCM analytically. By this reasonably simple approach presented in this study, significant reductions in the complexity and cost of the computations of jet impingement flow simulations are obtained. Furthermore, the effect of adding NEPCM

and nano-metal particles on the thermal performance of JIC can be easily investigated and interpreted.

2. Physical Model

2.1. Problem Description

The axisymmetric flow profile of a free-surface circular jet impinging with the velocity of v_j and the temperature of T_j is illustrated in Figure 1. As the circular jet impinges on the surface, flow is symmetrically diverted around the stagnation point and extends to the surface in a parallel manner. The primary mode of enhanced heat transfer is due to the flow stagnation in the stagnation region ($r < d_j/2$) [2,3]. Most JIC studies have investigated this region as the heat transfer enhancement is significant in this zone and continuously decreases with the distance away from the stagnation zone [1,3,4,18–20,32–34]. The present study also focuses on heat transfer in this region. Due to the balance between the stream acceleration (thinning boundary layer) and viscous diffusion (thickening boundary layer thickness), the boundary layer thickness is constant [35]. Boundary layer velocity (u) and freestream velocity (u_∞) profiles in r -direction are indicated in Figure 1.

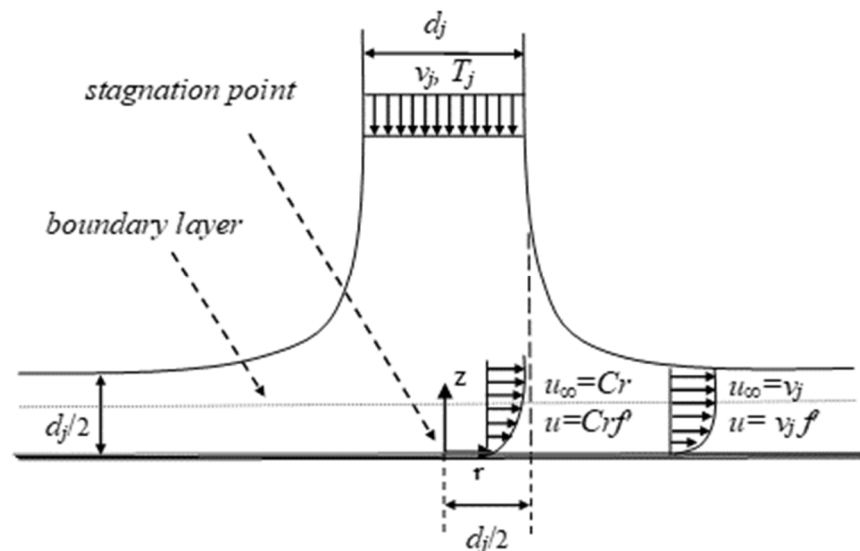


Figure 1. Axisymmetric stagnation flow profile of an impinging circular jet.

2.2. Mathematical Modeling

Considering a steady, axisymmetric, incompressible, laminar boundary layer flow and heat transfer of a viscous fluid in the neighborhood of a stagnation point on a flat plate located in $z = 0$, the conservation equations in cylindrical coordinates (r, z) with the corresponding velocity components (u, v) are presented as Equations (1)–(4):

Continuity equation:

$$\frac{\partial u}{\partial r} + \frac{u}{r} + \frac{\partial v}{\partial z} = 0 \quad (1)$$

r -momentum equation (radial direction):

$$u \frac{\partial u}{\partial r} + v \frac{\partial u}{\partial z} = -\frac{1}{\rho} \frac{\partial P}{\partial r} + \nu \left(\frac{\partial^2 u}{\partial r^2} + \frac{1}{r} \frac{\partial u}{\partial r} - \frac{u}{r^2} + \frac{\partial^2 u}{\partial z^2} \right) \quad (2)$$

z -momentum equation (axial direction):

$$u \frac{\partial v}{\partial r} + v \frac{\partial v}{\partial z} = -\frac{\partial P}{\partial z} + \nu \left(\frac{\partial^2 v}{\partial r^2} + \frac{1}{r} \frac{\partial v}{\partial r} + \frac{\partial^2 v}{\partial z^2} \right) \quad (3)$$

energy equation:

$$u \frac{\partial T}{\partial r} + v \frac{\partial T}{\partial z} = \alpha \left[\frac{1}{r} \frac{\partial}{\partial r} \left(r \frac{\partial T}{\partial r} \right) + \frac{\partial^2 T}{\partial z^2} \right] \quad (4)$$

In these equations, P and T represent the pressure and temperature fields, respectively. Parameters ρ , ν , and α are density, static viscosity, and thermal diffusivity of flow, respectively. Employing the Bernoulli's equation in the potential region, the following relations between free stream velocity $u_\infty(r)$ and the pressure gradients in r direction are specified:

$$-\frac{1}{\rho} \frac{\partial P}{\partial r} = u_\infty \frac{du_\infty}{dr} \quad (5)$$

The velocity components of the potential (inviscid) flow near the stagnation point are described as [27,35]:

$$u = -Cr \quad (6)$$

$$v = -2Cz \quad (7)$$

The C parameter represents the velocity gradient that is expressed in terms of the jet velocity and the jet diameter as $C = \bar{C} \frac{v_j}{d_j}$, where the value of $\bar{C} = 0.77$ for circular jet [36].

2.3. Similarity Solution

To convert partial differential Equations (1)–(4) into a set of ordinary differential equations, the following dimensionless similarity variables are introduced [3,27]:

$$\eta = \sqrt{\frac{C}{\nu}} z, \quad u = Cr f'(\eta), \quad v = -2\sqrt{C\nu} f(\eta), \quad \theta(\eta) = \frac{T - T_j}{\gamma}, \quad \text{where } \gamma = \frac{q''}{k} \sqrt{\frac{\nu}{C}} \quad (8)$$

Substituting these transformations into momentum and energy equations yields the following non-linear ordinary differential equations:

$$f''' + 2ff'' + 1 - f'^2 = 0 \quad (9)$$

$$\theta'' + 2Prf\theta' = 0 \quad (10)$$

where f and θ represent the dimensionless velocity and temperature in the boundary layer, respectively.

The boundary conditions correspondent to the above equations are as (form no slip and constant heat flux conditions on the wall):

$$\eta = 0 : \begin{cases} u = 0, v = 0, -k \frac{\partial T}{\partial z} \Big|_{z=0} = q'' \\ f' = f = 0, \theta' = -1 \end{cases} \quad (11)$$

$$\eta \rightarrow \infty : \begin{cases} u = u_\infty, T = T_j \\ f' = 1, \theta = 0 \end{cases} \quad (12)$$

The wall shear stress is defined as follows:

$$\tau_w = \mu \left(\frac{\partial u}{\partial z} + \frac{\partial v}{\partial r} \right) \Big|_{z=0} = \mu \left(Cr \sqrt{\frac{C}{\nu}} f''(0) \right) \quad (13)$$

Integrating Equation (13) over the stagnation zone, the averaged wall shear stress can be calculated by the following relation:

$$\tau_{w_{ave}} = \frac{1}{A} \int_0^{d_j/2} \tau_{w_{ave}} 2\pi r \cdot dr \quad (14)$$

where $A = \pi \frac{d_j^2}{4}$ is stagnation zone surface area. Subsuming Equation (13) into (14) and proper calculation, the averaged wall shear stress is calculated as follows:

$$\tau_{w_{ave}} = \frac{1}{3} \mu C d_j \sqrt{\frac{C}{\nu}} f''(0) \quad (15)$$

The heat transfer coefficient h is defined as follows:

$$h = \frac{q''}{T_w - T_j} \quad (16)$$

where T_w is the surface (wall) temperature. Using the dimensionless temperature variable form Equation (8) and substituting properly in Equation (16), the heat transfer coefficient can be calculated by the following relation:

$$h = k \sqrt{\frac{C}{\nu}} \frac{1}{\theta(0)} \quad (17)$$

Note that the flow properties in boundary layer are estimated in film temperature; $T_f = (T_w + T_j)/2$.

2.4. Thermophysical Properties Nano Particles and the Two-Phase Flow

Water is used as the base liquid coolant in the present study. The added nanoparticles to the base coolant are considered as nano capsules made up of polystyrene as shell and filled by n-octadecane paraffin wax as core (with the average size of 100 nm and 1:1 mixing ratio of wax to polymer), and metallic oxide aluminum (Al_2O_3) (with 30 nm average size) nanoparticles. The thermophysical properties of these components are listed in Table 1. The thermophysical properties of water listed in Table 1 are reported at the room temperature of 298.15 K; however, in the current simulations, the temperature-dependent properties are calculated and considered. The correlations to calculate the temperatures based on thermophysical properties of water are extracted from VDI-Heat Atlas [37].

As earlier mentioned, the single-phase flow approach which considers the effective properties of the mixture is employed to model the NEPCM slurry as well as nanofluid. The empirical correlations correspondent with the effective thermophysical properties NEPCM slurry and nanofluid, are summarized in Tables 2 and 3, respectively.

The melting process PCM happens in a temperature range. The full melting range (ΔT_m) of NEPCM particles is from 21.0 °C to 29.5 °C (T_1 and T_2 Table 2, respectively) [30]. Therefore, NEPCM particles are in a solid form in the temperatures less than T_1 and in liquid form for the temperature larger than T_2 . Within this range $\Delta T_m = T_2 - T_1$, phase change process happens and NEPCM particles absorb the heat in the form of latent heat. A sine profile in a proper resemblance to DSC curve suggested by Alisetti and Roy [38] is used in the present study.

Table 1. Thermophysical properties of coolant components [30,39].

Property (Unit)	Density; ρ (kg/m ³)	Specific Heat Capacity; c_p (J/kg K)	Thermal Conductivity; k (W/m K)	Latent Heat of Fusion; h_{sf} (J/kg)	Viscosity; μ (Pa.s)
Octadecane (solid)	850	1800	0.34	220.3	-
Octadecane (liquid)	780	2200	0.15	-	0.00385
NEPCM particles	1055	1965	0.22	107.1	-
Nano particles (Al_2O_3)	3880	773	36	-	-
Water (at 298.15 K)	997	4180	0.61	-	1.01

Table 2. The correlations to calculate the thermophysical properties of NEPCM slurry [40,41].

Effective Property	Correlations
Density (ρ_{eff})	$\varepsilon\rho_p + (1 - \varepsilon)\rho_w$
Specific heat capacity ($c_{p,eff}$)	$\varepsilon C_{p,p} + (1 - \varepsilon)C_{p,w}; C_{p,p} = C_{p,PCM} + \left[\frac{\pi}{2} \left(\frac{h_{sf}}{\Delta T_m} - C_{p,PCM} \right) \times \sin \left(\pi \frac{T - T_1}{\Delta T_m} \right) \right]$
Thermal conductivity (k_{eff})	$k_b(1 + B\varepsilon Pe_p^m); k_b = k_w \frac{2 + \frac{k_p}{k_w} + 2\varepsilon \left(\frac{k_p}{k_w} - 1 \right)}{2 + \frac{k_p}{k_w} - \varepsilon \left(\frac{k_p}{k_w} - 1 \right)}; Pe_p = \frac{eD_p}{\alpha_w};$ $e = \frac{1}{2} \xi_{ij} ; \begin{cases} Pe_p < 0.67 \rightarrow B = 3, m = 1.5 \\ 0.67 < Pe_p < 250 \rightarrow B = 1.8, m = 0.18 \\ Pe_p > 250 \rightarrow B = 3, m = 1/11 \end{cases}$
Viscosity (μ_{eff})	$\mu_w(1 - \varepsilon - 1.16\varepsilon^2)^{-2.5}$

Table 3. The correlations to calculate the thermophysical properties of nanofluid [39,42,43].

Effective Property	Correlations
Density (ρ_{eff})	$\varepsilon\rho_p + (1 - \varepsilon)\rho_w$
Specific heat capacity ($c_{p,eff}$)	$\frac{\varepsilon\rho_p c_{p,p} + (1 - \varepsilon)\rho_w c_{p,w}}{\rho_{eff}}$
Thermal conductivity (k_{eff})	$0.25 \left[(3\varepsilon - 1)k_p + (2 - 3\varepsilon)k_w + \sqrt{\Delta} \right]$ $\Delta = [(3\varepsilon - 1)k_p + (2 - 3\varepsilon)k_w]^2 + 8k_p k_w$
Viscosity (μ_{eff})	$\mu_w(123\varepsilon^2 + 7.3\varepsilon + 1)$

3. Numerical Solution

Equations (9) and (10) with the boundary conditions (11) and (12) are a set of highly nonlinear ordinary differential equations with boundary values. One of the most convenient and efficient methods to solve boundary value problems of a set of nonlinear ODEs is the fourth-order Runge–Kutta numerical method [6]. These boundary value problems have unknown parameters in the upper boundary condition (η_∞). So, the upper boundary conditions $f'(\infty)$, and $\theta(\infty)$ may be substituted by the initial boundary conditions $f''(0)$, and $\theta(0)$, to convert the boundary value problem to an initial value problem. For this purpose, the shooting technique is applied along with the fourth-order Runge–Kutta method with initial guesses for values $f''(0)$ and $\theta(0)$, and an iterative solution procedure till satisfying the upper boundary conditions $f'(\infty) = 1$ and $\theta(\infty) = 0$. The solution algorithm to obtain the dimensionless velocity and temperature field and finally the wall shear stress and the heat transfer coefficient is shown in a flowchart in Figure 2.

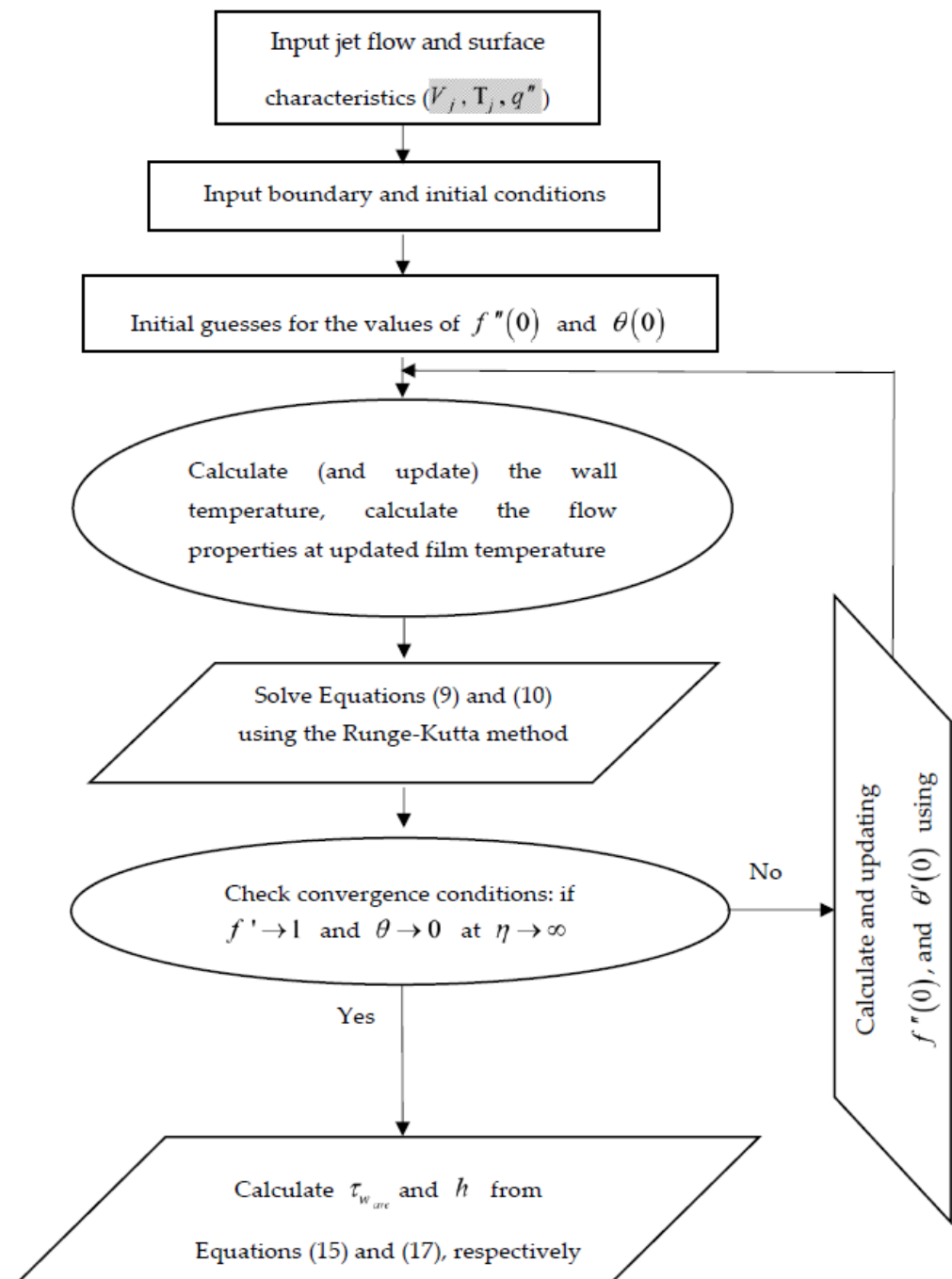


Figure 2. The flowchart for the numerical procedure.

4. Results and Discussion

The results obtained from the numerical integration of Equations (9) and (10) for the JIC problem under an arbitrary constant surface heat flux are plotted in Figure 3. Based on the boundary layer theory, the numerical solutions show that the dimensionless boundary layer thickness η_∞ is around 2 which coincides with results reported by [35].

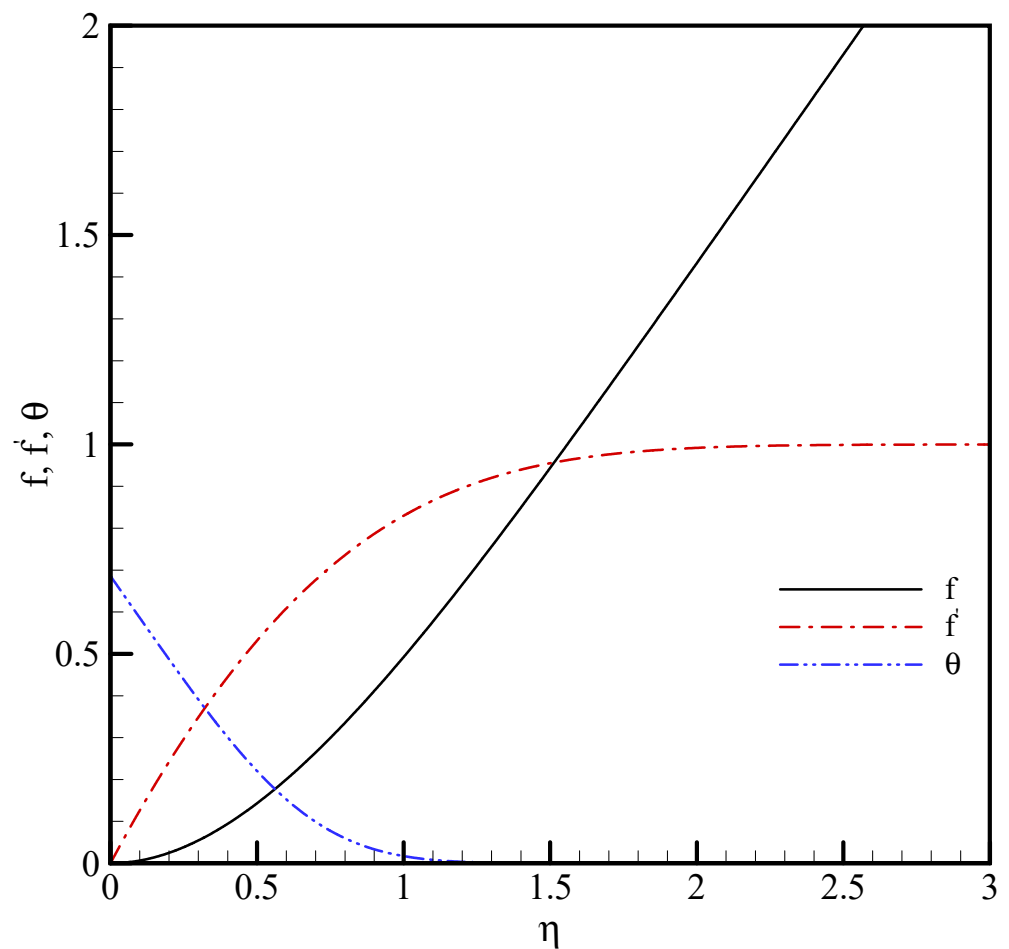


Figure 3. Dimensionless velocity (f , f') and temperature (θ) profiles in the stagnation region.

In the following, the main results from the analytical-numerical simulations to evaluate the heat transfer field and cooling performance of an impinging jet with the NEPCM slurry as coolant are presented. The nozzle and plate characteristics as well as NEPCM properties are conducted with the same physical, geometrical, and operating parameters reported by Wu et al. [30] as nozzle diameter (d_j), nozzle-to-surface distance (H), and constant heat flux (q'') and are set to 0.75 mm, 8 mm, and 30 W/cm², respectively. Furthermore, the results are assessed over a wide range of jet inlet velocity ($4 \text{ m/s} \leq V_j \leq 16$), jet inlet temperature ($16 \text{ }^\circ\text{C} \leq T_j \leq 32 \text{ }^\circ\text{C}$), NEPCM particle volume concentration ($0 \leq \varepsilon \leq 0.3$), and alumina nanoparticle concentration ($0 \leq \phi \leq 0.06$). In order to validate the results presented in this paper, the heat transfer coefficient results obtained from the current model are compared with the results obtained from an experiment-based correlation for water jet reported by Liu et al. [36] (Figure 4). For the case of NEPCM slurry jet, Nu number results are compared with the experimental results conducted by [30] for a special case of 28% particle volume fraction (Figure 5). As can be seen, a very good agreement for both cases is reported.

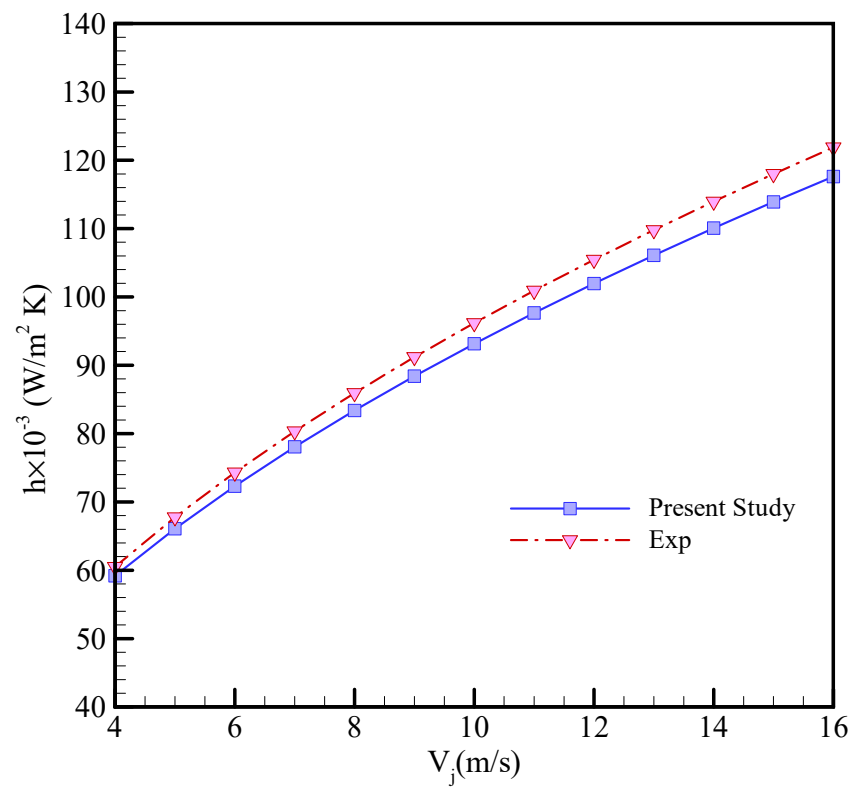


Figure 4. Numerical model validation by comparing with the results reported by [36] for water as coolant.

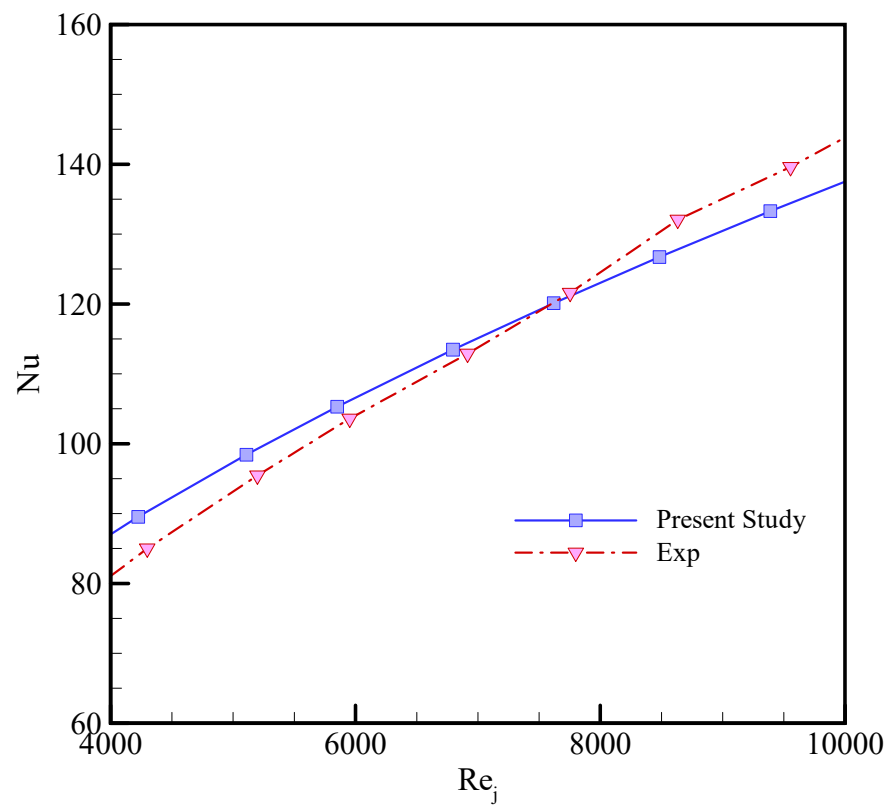


Figure 5. Numerical model validation by comparing with the results reported by [36] for NEPCM slurry (with 28% particle volume fraction) as coolant.

Zhang and Faghri [40] observed that NEPCM slurry behaves as Newtonian fluid for particle volume fraction below 0.3. Therefore, in the present study, NEPCM slurries with particle volume fractions below 0.3 are considered to be treated as a Newtonian fluid. Nanoparticles dispersed in water will influence the hydrodynamic of the fluid flow, such as viscosity of the flow and shear stresses as a result of the relative motion between the nanoparticles and the liquid flow. Figure 6 shows the effect of NEPCM concentration on the variation of the average wall shear stress of stagnation flow with respect to Re number. Shear stress increases with the increase of Re as expected. At the same Re number, NEPCM slurry reports higher wall shear stresses compared with water and also with the increasing concentration of NEPCM, shear stresses grow significantly due to higher effective viscosity.

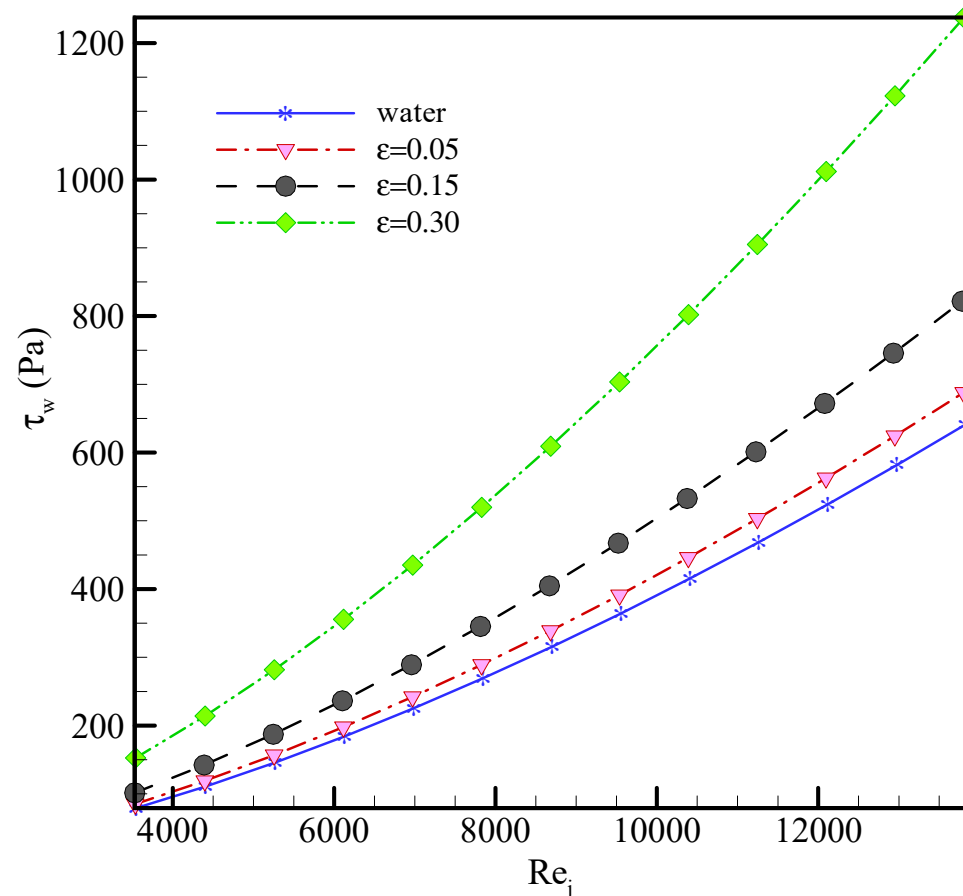


Figure 6. The effect of NEPCM concentration on the average wall shear stress of stagnation flow as function of Re number.

As JIC is aimed to heat transfer applications, the rest of the results focus on the heat transfer parameters and their effect on the thermal performance of the JIC. Figure 7 shows the effect of particle volume fraction of NEPCM slurry on the distribution of the dimensionless temperature (θ profiles) in the boundary layer thickness. As expected from the similarity solution, the trend of all profiles is the same (general profile), but the effect of NEPCM concentration is significant on the values at the surface (at $\eta = 0$) and the thickness of the thermal boundary layer ($\eta_\infty = \delta_T$). As heat flux is transferred through the wall, we are interested in the thermal field values on the surface. According to Equations (9) and (10), the dimensionless temperature in the boundary layer only depends on Pr number. Therefore, the effect of the NEPCM concentration is exerted on the temperature field/equation through Pr number. The value of dimensionless temperature at the surface; $\theta(0)$ and its variation with respect to Pr number and NEPCM concentration in the slurry jet is depicted in Figure 8. As seen, $\theta(0)$ decreases with the increasing NEPCM concentration (and therefore Pr number). According to Equation (16), decreasing $\theta(0)$ should

lead to an increase in heat transfer coefficient. However, in addition to dimensionless temperature at the surface; $\theta(0)$, the heat transfer coefficient depends also on some other characteristics of fluid flow (C) and thermal (k & ν) fields.

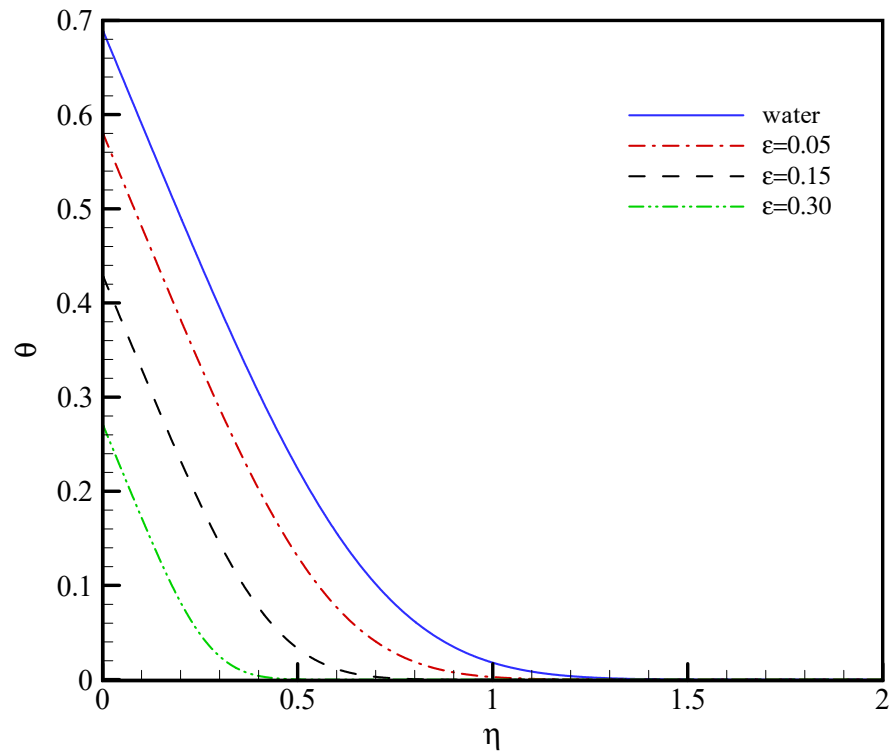


Figure 7. The effect of particle volume fraction of NEPCM slurry on the dimensionless temperature profiles in boundary layer.

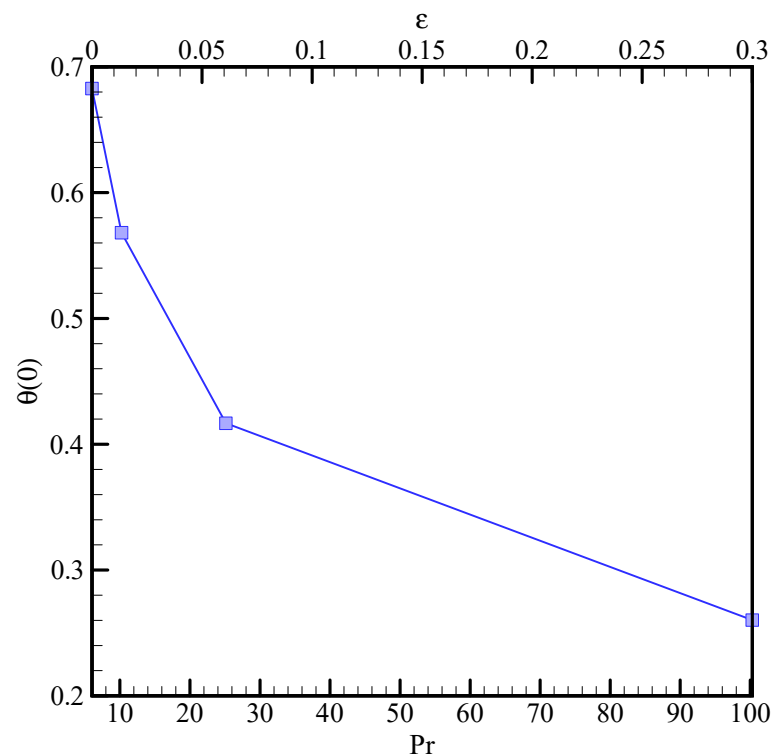


Figure 8. The variation of dimensionless temperature at the surface ($\eta = 0$) with respect to Pr number as well as particle volume fraction of NEPCM slurry.

The comparison of jet impingement heat transfer coefficients for the NEPCM slurry with different particle volume fraction at inlet jet temperatures of 25 °C as a function of jet velocity which varies from 4 to 16 m/s (flow rate from 1.8 to 7.3 g/s) is illustrated in Figure 9.

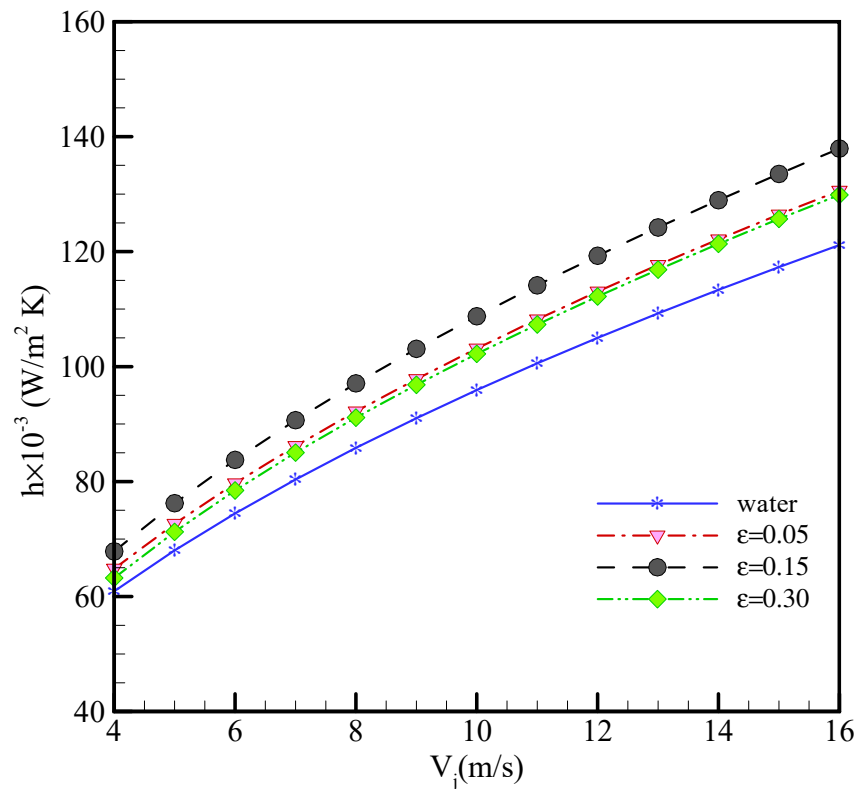


Figure 9. The variation of heat transfer coefficients with respect to jet velocity for NEPCM slurry with different particle volume fraction when the inlet jet temperature is set at 25 °C.

As seen for all test cases, a higher flow rate (or inlet jet velocity) increases a higher heat transfer coefficient and therefore cooling rate and vice versa. The figure also indicates that for this specific inlet temperature, apart from the NEPCM concentration value, the slurry jet has a higher heat transfer performance compared with the pure water jet due to absorbing heat flux as the latent heat and therefore the wall temperature rising slows down. However, the results show that slurry with a 15% particle volume fraction has the highest heat transfer coefficients among others. Adding more NEPCM particles to the slurry would decrease the cooling performance.

It is interesting to find under what conditions the cooling performance is the maximum. For this purpose, the heat flux and jet velocity (mass flow rate) are set to 30 W/cm² and 8 m/s (3.6 g/s), respectively, while the jet inlet temperature and NEPCM concentration are varied between 16 and 32 °C, and 0 to 0.4, respectively. First, the comparison of transfer coefficient profiles as a function of inlet jet temperature for water and NEPCM slurry with different particle volume fractions is provided in Figure 10. Except for the case of the water jet which has a slight increasing slope, the profiles regarding slurry jets have a peak within the melting temperature range of PCM. Within this range, PCM starts to melt and therefore the heat transfer coefficients increase. For a heated surface at a temperature out of the melting range, water has a higher heat transfer coefficient. This is because, as shown earlier, with increasing particle volume fraction in slurry, viscosity sharply increases. This increase will thicken the boundary layer and hence will reduce the heat transfer as a result. Therefore, the overall heat transfer coefficient decreases. Furthermore, for the lower inlet temperatures ($T_j < 19$ °C), there would be no phase change, and the heat transfer coefficient for slurry is lower than for the water case, because the slurry has a lower conductivity than water as a result of the lower conductivity of NEPC particles.

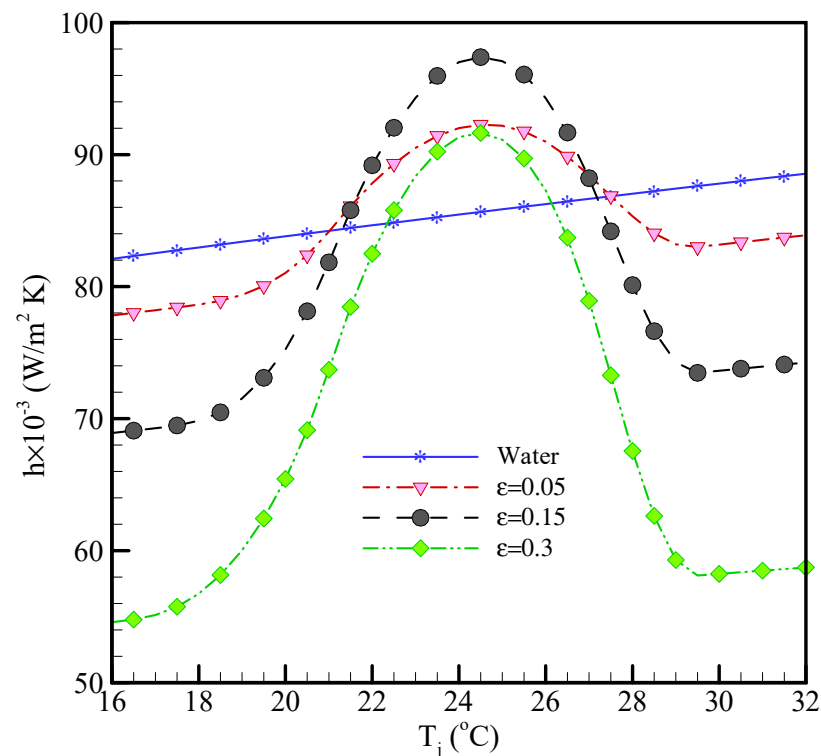


Figure 10. Heat transfer coefficient profiles as function of inlet jet temperature for water and NEPCM slurry with different particle volume fraction ($V_j = 8$ m/s).

The results also indicate that the maximum enhancement in the heat transfer coefficient for slurry cases occurred at an inlet jet temperature of 25.2, which is quite close to the peak temperature (26.2) measured by DSC melting curve [30]. Furthermore, this peak has the maximum value at the particle volume fraction of 15%. To find the optimum particle volume fraction corresponding with the maximum value over a wider and continuous range, the variation of heat transfer coefficients versus particle volume fraction is depicted in Figure 11. As can be seen, the curves have a peak in $\epsilon = 0.15$ and this concentration is not varied with the jet velocity/flow rate.

To investigate the effect of nanoparticles on the cooling performance of the JIC and compare the results with ones for the water and slurry jets, the heat transfer coefficients for the nanofluid jet impingement are also calculated. The variation of heat transfer coefficients with respect to jet velocity for three different particle volume fractions at inlet jet temperatures of 25 °C is depicted and compared with water in Figure 12. As seen, increasing nanoparticle concentration will slightly increase the heat transfer coefficient, but the effect seems less significant compared to the results found for adding the NEPCM particles in Figure 9. Tang et al. [44] conducted an experimental work on Al_2O_3 nanofluids to characterize the viscosity and shear stresses. They found that alumina nanoparticles dispersed below 6% volume concentration exhibit Newtonian behavior for an operating temperature range from 6 to 75 °C. Therefore, nanofluids below 6% are assumed to be Newtonian fluid. Figure 13 compares the heat transfer coefficients for water, nanofluid, and NEPCM slurry jets for particle concentrations, leading to the maximum value for the heat transfer. As seen, at the same jet velocity, the maximum heat transfer coefficients for NEPCM slurry are significantly higher than those for nanofluid. Compared with the water jet, adding NEPCM and nanoparticles would overall enhance the thermal performance of the JIC by 16% and 7%, respectively.

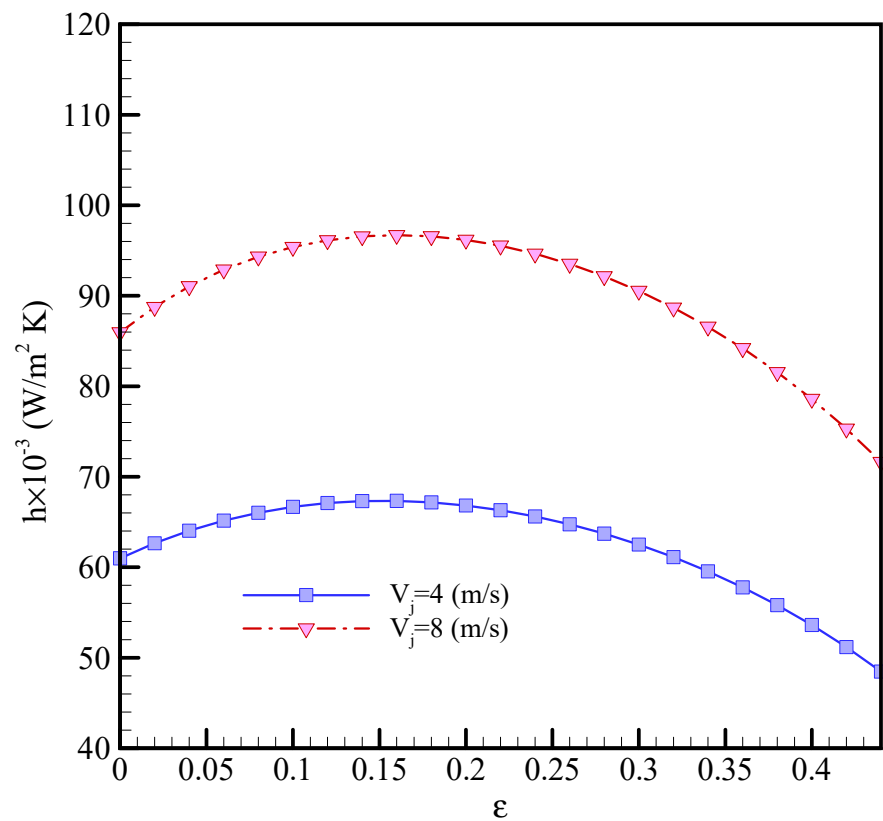


Figure 11. The variation of heat transfer coefficients as function of particle volume fraction for the two different jet velocities.

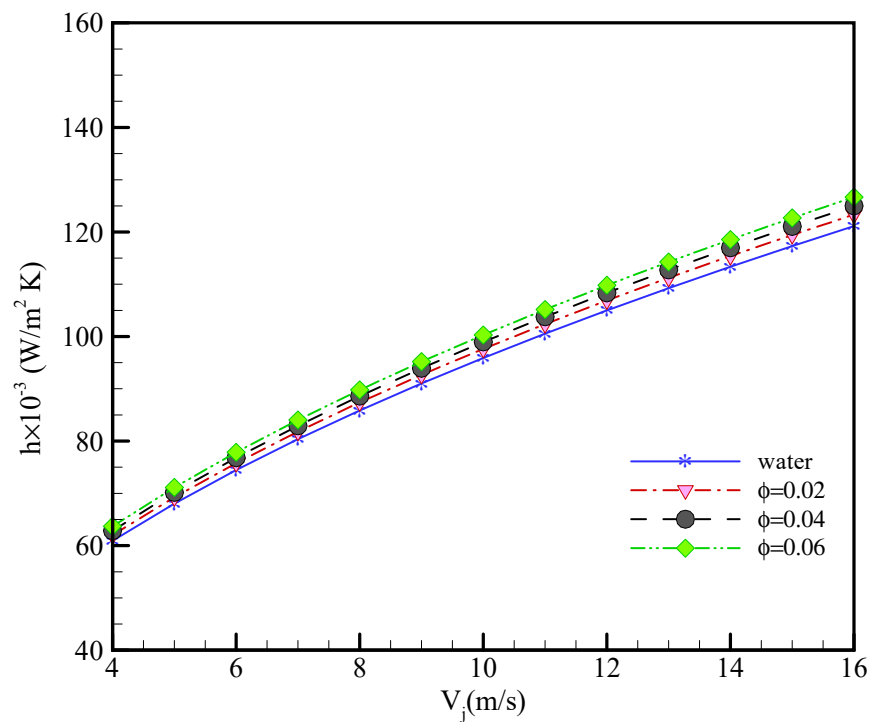


Figure 12. The variation of heat transfer coefficients with respect to jet velocity for nanofluid with different particle volume fraction ($T_j = 25\text{ }^\circ\text{C}$).

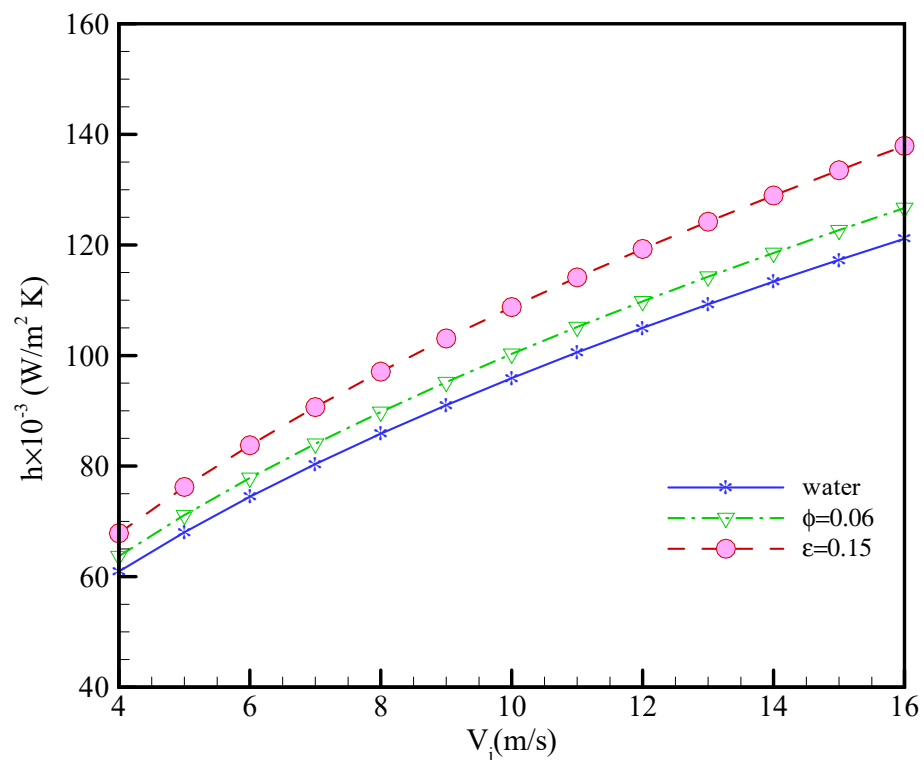


Figure 13. Comparison of the heat transfer coefficients for water, nanofluid, and NEPCM slurry jets as a function of jet velocity.

5. Conclusions

In this paper, the flow and the heat transfer of free-surface jet impingement cooling using water, NEPCM slurry, and nanofluid were studied. An analytical solution using a similarity approach was presented to determine the main characteristics of flow and heat transfer fields, such as the wall shear stress and the heat transfer coefficient. The effect of NEPCM particle concentration on these characteristics was investigated. It was found that wall shear stress significantly increases with the increase of NEPCM concentration. Furthermore, adding NEPCM particles to the water jet can be effective if the inlet temperature is in the range of the melting temperature of the utilized PCM. Moreover, there was an optimum value for the particle concentration that led to maximizing the heat transfer coefficient of JIC. It was also found that in the maximum performance, NEPCM slurry shows a better result compared to the nanofluid as it enhanced the thermal performance of the system by 16%, while the nanofluid enhances the performance by 7%, compared with water. However, the maximum performance of the NEPCM slurry strongly depends on the inlet jet temperature and volume concentration. At the inlet temperature of 25.2 °C and concentration of 15%, the maximum performance is achieved. It is suggested that the future work focus should be on the NEPCM particles with higher latent heat and especially higher thermal conductivity to overcome the weakness of NEPCM slurries.

Author Contributions: Conceptualization, M.R.M. and S.M.; methodology, M.R.M.; software, M.R.M.; validation, M.R.M., and S.M.; formal analysis, M.R.M. and A.A.A.; investigation, M.R.M.; resources, M.R.M.; data curation, M.R.M.; writing—original draft preparation, M.R.M.; writing—review and editing, M.R.M., A.A.A., S.H.T., and S.M.; visualization, M.R.M.; supervision, S.M.; project administration, S.M.; funding acquisition, S.M. All authors have read and agreed to the published version of the manuscript.

Funding: This research was funded by the Discovery Grant from NSERC (Natural Sciences and Engineering Research Council) Canada grant number [401495]. The APC was funded by [Author Voucher discount code (91df8599292d61dc)].

Institutional Review Board Statement: Not applicable.

Informed Consent Statement: Not applicable.

Data Availability Statement: Not applicable.

Conflicts of Interest: The authors declare no conflict of interest.

Nomenclature

C	velocity gradient [S^{-1}]
c_p	specific heat [$J/kg\ K$]
d_j	Nozzle diameter [m or mm]
f	Dimensionless velocity
h	convective heat transfer coefficient [$W/m^2\ K$]
h_{sf}	latent heat of fusion [J/kg]
k	thermal conductivity [$W/m\ K$]
P	Pressure [Pa]
Pr	Prandtl number
q''	Wall heat flux [W/m^2]
r	Cartesian coordinate, [m or mm]
Re	Reynolds number
T	temperature [$^{\circ}C$ or K]
ΔT	temperature difference [$^{\circ}C$ or K]
u	velocity component in r direction [m/s]
v	velocity component in z direction [m/s]
v_j	Inlet jet velocity
z	Cartesian coordinate, [m or mm]
Greek symbols	
α	Thermal diffusivity [m^2/s]
θ	Dimensionless temperature
ν	Kinematic viscosity [m^2/s]
ε	Volume fraction of NEPCM particle
φ	Volume fraction of nanoparticles
τ_w	Wall shear stress
μ	Dynamic viscosity [$Pa.s$]
ρ	density [kg/m^3]
η	Dimensionless coordinate/length
Subscripts	
b	Bulk
eff	Effective Property
j	Jet related
l	liquid PCM
m	melt
p	Particle
s	solid PCM
w	Wall/Water related
∞	Potential (inviscid) flow related
Abbreviation	
JIC	Jet impingement cooling
MF	Melt fraction
Nu	Nusselt number
PCM	Phase change material
NEPCM	Nano-encapsulated phase change material

References

1. Mohaghegh, M.R.; Rahimi, A.B. Single- and two-phase water jet impingement heat transfer on a hot moving surface. *J. Therm. Anal. Calorim.* **2019**, *137*, 1401–1411. [[CrossRef](#)]
2. Ekkad, S.V.; Singh, P. A Modern Review on Jet Impingement Heat Transfer Methods. *J. Heat Transf.* **2021**, *143*, 064001. [[CrossRef](#)]

3. Mohaghegh, M.R.; Rahimi, A.B. Modeling of nucleate boiling heat transfer of a stagnation-point flow impinging on a hot surface. *Therm. Sci.* **2019**, *23*, 695–706. [[CrossRef](#)]
4. Wolf, D.; Incropera, F.; Viskanta, R. Jet Impingement Boiling. *Adv. Heat Transf.* **1993**, *23*, 1–132.
5. Zuckerman, N.; Lior, N. Jet impingement heat transfer: Physics, correlations, and numerical modeling. *Adv. Heat Transf.* **2006**, *39*, 565–631.
6. Mohaghegh, M.; Rahimi, A.B.; Mahmud, S. Non-axisymmetric three-dimensional stagnation-point flow and heat transfer under a jet impingement boiling. *J. Therm. Anal. Calorim.* **2021**, *145*, 211–224. [[CrossRef](#)]
7. Glynn, C.; O'Donovan, T.; Murray, D.B.; Feidt, M. Jet impingement cooling. In Proceedings of the 9th UK National Heat Transfer Conference, Manchester, UK, 5–6 September 2005; pp. 5–6.
8. Lienhard, J. Liquid Jet Impingement. *Annu. Rev. Heat Transf.* **1995**, *6*, 199–270. [[CrossRef](#)]
9. Wolf, D.H.; Viskanta, R.; Incropera, F.P. Turbulence Dissipation in a Free-Surface Jet of Water and Its Effect on Local Impingement Heat Transfer From a Heated Surface: Part 2—Local Heat Transfer. *J. Heat Transf.* **1995**, *117*, 95–103. [[CrossRef](#)]
10. Zuckerman, N.; Lior, N. Impingement Heat Transfer: Correlations and Numerical Modeling. *J. Heat Transf.* **2005**, *127*, 544–552. [[CrossRef](#)]
11. Shokrgozar Abbasi, A.; Bradaran Rahimi, A.; Niazmand, H. Exact solution of three-dimensional unsteady stagnation flow on a heated plate. *J. Thermophys. Heat Transf.* **2011**, *25*, 55–58. [[CrossRef](#)]
12. Shokrgozar Abbasi, A.; Baradaran Rahimi, A. Investigation of Two-Dimensional Unsteady Stagnation-Point Flow and Heat Transfer Impinging on an Accelerated Flat Plate. *J. Heat Transf.* **2012**, *134*, 064501. [[CrossRef](#)]
13. Wang, B.; Guo, X.; Xie, Q.; Wang, Z.; Wang, G. Heat Transfer Characteristic Research during Jet Impinging on Top/Bottom Hot Steel Plate. *Int. J. Heat Mass Transf.* **2016**, *101*, 844–851. [[CrossRef](#)]
14. Hadipour, A.; Rajabi Zargarabadi, M.; Dehghan, M. Effect of micro-pin characteristics on flow and heat transfer by a circular jet impinging to the flat surface. *J. Therm. Anal. Calorim.* **2020**, *140*, 943–951. [[CrossRef](#)]
15. Matheswaran, M.M.; Arjunan, T.V.; Somasundaram, D. Analytical investigation of exergetic performance on jet impingement solar air heater with multiple arc protrusion obstacles. *J. Therm. Anal. Calorim.* **2019**, *137*, 253–266. [[CrossRef](#)]
16. Nawani, S.; Subhash, M. A review on multiple liquid jet impingement onto flat plate. *Mater. Today Proc.* **2021**, *46*, 11190–11197. [[CrossRef](#)]
17. Miyasaka, Y.; Inada, S. The Effect of Pure Forced Convection on the Boiling Heat Transfer between a Two-Dimensional Subcooled Water Jet and a Heated Surface. *J. Chem. Eng. Jpn.* **1980**, *13*, 22–28. [[CrossRef](#)]
18. Wolf, D.; Incropera, F.; Viskanta, R. Local Jet Impingement Boiling Heat Transfer. *Int. J. Heat Mass Transf.* **1996**, *39*, 1395–1406. [[CrossRef](#)]
19. Hall, D.E.; Incropera, F.P.; Viskanta, R. Jet Impingement Boiling from a Circular Free-Surface Jet during Quenching: Part 2—Two-Phase Jet. *J. Heat Transf.* **2001**, *123*, 911–917. [[CrossRef](#)]
20. Robidou, H.; Auracher, H.; Gardin, P.; Lebouche, M.; Bogdanić, L. Local Heat Transfer from a Hot Plate to a Water Jet. *Heat Mass Transf.* **2003**, *39*, 861–867. [[CrossRef](#)]
21. Karwa, N.; Gambaryan-Roisman, T.; Stephan, P.; Tropea, C. Experimental Investigation of Circular Free-Surface Jet Impingement Quenching: Transient Hydrodynamics and Heat Transfer. *Exp. Therm. Fluid Sci.* **2011**, *35*, 1435–1443. [[CrossRef](#)]
22. Li, Y.-Y.; Liu, Z.-H.; Wang, Q. Experimental Study on Critical Heat Flux of Steady Boiling for High-Velocity Slot Jet Impinging on the Stagnation Zone. *Int. J. Heat Mass Transf.* **2014**, *70*, 1–9. [[CrossRef](#)]
23. Modak, M.; Nirgude, V.; Sharma, A.K.; Sahu, S.K. Experimental Study on Heat Transfer Characteristics of Circular Jet Impingement Boiling on the Variety of Structured Copper Surfaces in Stagnation Zone. In *International Conference on Nuclear Engineering*; American Society of Mechanical Engineers: Charlotte, NC, USA, 2016; p. V005T15A048. [[CrossRef](#)]
24. Karimi Kerdabadi, J.; Haghaniimesh, M.; Karimipour, A.; Toghraie, D.; Tlili, I. The experimental/numerical investigation of variations in strip speed, water shower pattern and water temperature on high-temperature strip cooling rate in hot strip mill. *J. Therm. Anal. Calorim.* **2020**, *143*, 293–308. [[CrossRef](#)]
25. Shafee, A.; Rezaeianjouybari, B.; Sheikholeslami, M.; Allahyari, M.; Babazadeh, H. Boiling process with incorporating nanoparticles through a flattened channel using experimental approach. *J. Therm. Anal. Calorim.* **2020**, *143*, 3569–3576. [[CrossRef](#)]
26. Sheikholeslami, M.; Rezaeianjouybari, B.; Darzi, M.; Shafee, A.; Li, Z.; Nguyen, T.K. Application of nano-refrigerant for boiling heat transfer enhancement employing an experimental study. *Int. J. Heat Mass Transf.* **2019**, *141*, 974–980. [[CrossRef](#)]
27. Mohaghegh, M.; Rahimi, A.B. Three-dimensional stagnation-point flow and heat transfer of a dusty fluid toward a stretching sheet. *J. Heat Transf.* **2016**, *138*, 112001. [[CrossRef](#)]
28. Tyagi, P.K.; Kumar, R.; Mondal, P.K. A review of the state-of-the-art nanofluid spray and jet impingement cooling. *Phys. Fluids* **2020**, *32*, 121301. [[CrossRef](#)]
29. Rajabifar, B. Enhancement of the performance of a double layered microchannel heatsink using PCM slurry and nanofluid coolants. *Int. J. Heat Mass Transf.* **2015**, *88*, 627–635. [[CrossRef](#)]
30. Wu, W.; Bostanci, H.; Chow, L.; Ding, S.; Hong, Y.; Su, M.; Kizito, J.P.; Gschwender, L.; Snyder, C. Jet impingement and spray cooling using slurry of nanoencapsulated phase change materials. *Int. J. Heat Mass Transf.* **2011**, *54*, 2715–2723. [[CrossRef](#)]
31. Rehman, M.M.U.; Qu, Z.; Fu, R.; Xu, H. Numerical study on free-surface jet impingement cooling with nanoencapsulated phase-change material slurry and nanofluid. *Int. J. Heat Mass Transf.* **2017**, *109*, 312–325. [[CrossRef](#)]

32. Vader, D.; Incropera, F.; Viskanta, R. Convective Nucleate Boiling on a Heated Surface Cooled by an Impinging, Planar Jet of Water. *J. Heat Transf.* **1992**, *114*, 152–160. [[CrossRef](#)]
33. Omar, A.; Hamed, M.; Shoukri, M. Modeling of Nucleate Boiling Heat Transfer under an Impinging Free Jet. *Int. J. Heat Mass Transf.* **2009**, *52*, 5557–5566. [[CrossRef](#)]
34. Timm, W.; Weinzierl, K.; Leipertz, A. Heat Transfer in Subcooled Jet Impingement Boiling at High Wall Temperatures. *Int. J. Heat Mass Transf.* **2003**, *46*, 1385–1393. [[CrossRef](#)]
35. White, F.M. *Viscous Fluid Flow*, 3rd ed.; McGraw-Hill: New York, NY, USA, 2006.
36. Liu, X.; Gabour, L.A.; Lienhard, V.J.H. Stagnation-Point Heat Transfer during Impingement of Laminar Liquid Jets: Analysis Including Surface Tension. *J. Heat Transf.* **1993**, *115*, 99–105. [[CrossRef](#)]
37. Kleiber, M.; Joh, R.; Span, R. D3 properties of pure fluid substances. In *VDI Heat Atlas*; Springer: Berlin/Heidelberg, Germany; Dusseldorf, Germany, 2010.
38. Alisetti, E.L.; Roy, S.K. Forced convection heat transfer to phase change material slurries in circular ducts. *J. Thermophys. Heat Transf.* **2000**, *14*, 115–118. [[CrossRef](#)]
39. Li, P.; Zhang, D.; Xie, Y. Heat transfer and flow analysis of Al₂O₃–water nanofluids in microchannel with dimple and protrusion. *Int. J. Heat Mass Transf.* **2014**, *73*, 456–467. [[CrossRef](#)]
40. Zhang, Y.; Faghri, A. Analysis of forced convection heat transfer in microencapsulated phase change material suspensions. *J. Thermophys. Heat Transf.* **1995**, *9*, 727–732. [[CrossRef](#)]
41. Charunyakorn, P.; Sengupta, S.; Roy, S. Forced convection heat transfer in microencapsulated phase change material slurries: Flow in circular ducts. *Int. J. Heat Mass Transf.* **1991**, *34*, 819–833. [[CrossRef](#)]
42. Maiga, S.E.B.; Palm, S.J.; Nguyen, C.T.; Roy, G.; Galanis, N. Heat transfer enhancement by using nanofluids in forced convection flows. *Int. J. Heat Fluid Flow* **2005**, *26*, 530–546. [[CrossRef](#)]
43. Vajjha, R.S.; Das, D.K. Experimental determination of thermal conductivity of three nanofluids and development of new correlations. *Int. J. Heat Mass Transf.* **2009**, *52*, 4675–4682. [[CrossRef](#)]
44. Tang, C.C.; Tiwari, S.; Cox, M.W. Viscosity and friction factor of aluminum oxide–water nanofluid flow in circular tubes. *J. Nanotechnol. Eng. Med.* **2013**, *4*, 021004. [[CrossRef](#)]